


 Cite this: *Chem. Commun.*, 2021, 57, 7926

 Received 22nd June 2021,
 Accepted 13th July 2021

DOI: 10.1039/d1cc03311e

rsc.li/chemcomm

Crystallization-induced emission enhancement of highly electron-deficient dicyanomethylene-bridged triarylboranes†

 Guanming Liao,^{ab} Jia Zhang,^a Xiaoyan Zheng,^{id} *^a Xiaodi Jia,^c Jialiang Xu,^{id} ^c Fenggui Zhao,^a Nan Wang,^{id} ^a Kanglei Liu,^a Pangkuan Chen^{id} *^a and Xiaodong Yin^{id} *^a

A highly electron-deficient dicyanomethylene-bridged triarylborane, ^FMesB-TCN, was reported with a low-lying LUMO and crystallization-induced emission enhancement in its block-shape crystal. DFT calculations revealed lower re-organization energy of the block crystal than that of the weakly emissive acicular crystal. This work explored a novel boron-containing skeleton with interesting optical properties.

Molecular aggregates with unique optical and electronic properties are of great importance for real-world applications.^{1–10} Among them, organic crystalline materials have drawn considerable attention due to their potential applications in the area of organic field effect transistors and solid state lasers.^{11,12} The emission enhancement observed in the aggregated state was coined aggregation induced emission (AIE) by Tang and co-workers.^{13,14} As one of the branches of AIE, crystallization-induced emission enhancement (CIEE) is a unique photophysical phenomenon in which the compound emits weakly in the amorphous or solution state but becomes strongly emissive in crystalline states.¹⁵ Until now, a few developments in CIEE based on organic compounds have been achieved.^{16–20} Tang *et al.* reported a diphenylacetylene derivative with fluorescence quantum efficiency changes from low ($\Phi_F = 0.09$) to evidently enhanced ($\Phi_F = 0.6$) in the amorphous solid and crystal state, respectively.¹⁶ Chujo *et al.* reported a novel anthracene-*o*-carborane dyad with both AIE and CIEE character with the quantum yield increasing from the solution in THF ($\Phi_F = 0.02$) to

aggregation ($\Phi_F = 0.18$) and the crystal ($\Phi_F = 0.38$).¹⁷ Gu *et al.* reported squaraines (SQs) which showed weak emission in solution while relatively strong in the crystal state. Furthermore, co-crystallization between CIEE-SQ and chloroform induces dramatic emission enhancement, with about a 10-fold increase of the emission efficiency and a slight blue shift.¹⁸ Inspired by these, triarylboranes with tunable solid-state emission are envisioned to develop novel CIEE systems. Herein, we report the synthesis of a series of highly electron-deficient dicyanomethylene-bridged triarylboranes with a significant CIEE phenomenon observed in the block crystal of ^FMesB-TCN, which exhibits a much higher photo-luminescence quantum yield ($\Phi_F = 0.33$) than that of the solution state and neat film ($\Phi_F = 0.01$).

The synthesis of ^FMesB-TCN and Mes*B-TCN is described in detail in the ESI.† 5,5-Dimethyl-5,12-dihydrobenzo[*b*]naphtho[2,3-*e*]stannine (TT) was prepared according to the reported procedure by the Piers group.²¹ As shown in Fig. 1a, TT was treated with BCl₃ to obtain the chloroborane (Cl-BT), which was used for the next step without purification beyond removal of the solvent and the Me₂SnCl₂ byproduct. The reaction of Cl-BT with ^FMes-Li and Mes*B-Li in toluene generated ^FMesB-T and Mes*B-T with reasonable yields, respectively. Oxidation of ^FMesB-T and Mes*B-T with CrO₃ in refluxing acetic acid produced carbonyl-functionalized triarylboranes ^FMesB-TQ and Mes*B-TQ. Finally, the carbonyl functionalities were transformed to dicyanomethylene groups under Knoevenagel conditions to yield ^FMesB-TCN (55%) and Mes*B-TCN (50%). These products exhibited sufficient stability and could be purified by column chromatography on silica gel in an ambient atmosphere without noticeable decomposition.

Single crystals of the ^FMes- and Mes*-substituted triarylborane were obtained by slow evaporation of hexane/dichloromethane solutions. The structures of these compounds were verified by X-ray crystallographic analyses (Fig. 1b and Fig. S1, ESI†). Selected bond lengths and angles are listed in Table S3 (ESI†). The central boron atom of these molecules adopts a trigonal planar geometry. It's noteworthy that the dihedral angles between the two fused benzene/naphthalene rings of the dicyanomethylene-functionalized compounds are 28.76° for

^a Key Laboratory of Cluster Science, Ministry of Education of China, Beijing Key Laboratory of Photoelectronic/Electrophotonic Conversion Materials, School of Chemistry and Chemical Engineering, Beijing Institute of Technology, Beijing, 102488, P. R. China. E-mail: yinxid18@bit.edu.cn, pangkuan@bit.edu.cn, xiaoyanzheng@bit.edu.cn

^b School of Chemistry and Chemical Engineering, Jiangxi Science and Technology Normal University, Nanchang, Jiangxi, 330013, P. R. China

^c School of Materials Science and Engineering, National Institute for Advanced Materials, Nankai University, Tongyan Road 38, Tianjin, 300350, P. R. China

† Electronic supplementary information (ESI) available: Synthetic routes, data of single crystal structures, characterization data, and DFT calculation data. CCDC 2010873, 2013631, 2013632, 2082134, 2081903, 2086880 and 2086881. For ESI and crystallographic data in CIF or other electronic format see DOI: 10.1039/d1cc03311e

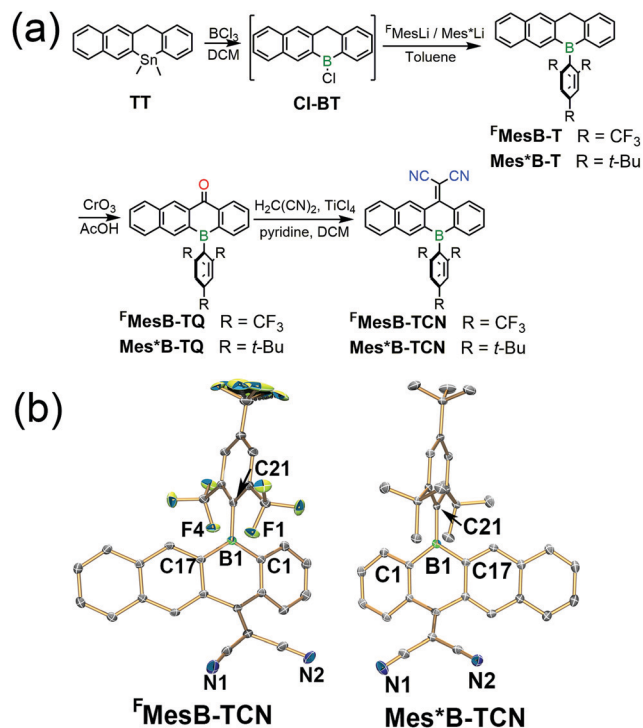


Fig. 1 (a) Synthesis routes of dicyanomethylene-functionalized triarylboranes; and (b) X-ray structure plots of $^{\text{F}}\text{MesB-TCN}$ and $\text{Mes}^*\text{B-TCN}$ with thermal ellipsoids drawn at 50% probability.

$^{\text{F}}\text{MesB-TCN}$ and 26.20° for $\text{Mes}^*\text{B-TCN}$, revealing a non-planar “butterfly” structure due to the steric hindrance between the dicyanomethylene moieties and the boratetracene skeleton. The B–F distances of 2.510 and 2.645 Å for $^{\text{F}}\text{MesB-TCN}$ are much shorter than the sum of the B and F van der Waals radii of 3.39 Å,²² indicating the weak interaction between boron and fluorine atoms.

The photophysical properties of the carbonyl- and dicyanomethylene-functionalized compounds were recorded in THF (Fig. 2a). The absorption spectrum displayed a broad band, which covered the region from 220 nm to 470 nm. A slight redshift in the absorption of the dicyanomethylene-functionalized derivatives compared to the carbonyl-bridged compounds can be observed, confirming the influence of the more electron-deficient group. The electrochemical properties of the $^{\text{F}}\text{Mes}$ - and Mes^* -substituted triarylborane were examined by cyclic voltammetry in CH_2Cl_2 and THF, respectively (Fig. 2b and Fig. S7 and Table S6, ESI[†]). In the carbonyl-bridged triarylboranes, the first reversible reduction waves were observed at $E_{1/2} = -1.51$ ($^{\text{F}}\text{MesB-TQ}$) and -1.81 V ($\text{Mes}^*\text{B-TQ}$) vs. $\text{Fc}^{+/0}$. The dicyanomethylene derivatives $^{\text{F}}\text{MesB-TCN}$ and $\text{Mes}^*\text{B-TCN}$ show relatively positive reduction potentials at ca. -1.19 V and -1.33 V, respectively (Table 1). Then the LUMO energy levels of these compounds can be estimated with the equation of $E_{\text{LUMO}} = -(4.8 + E_{\text{red}})$ to obtain the lowest LUMO at -3.61 eV for $^{\text{F}}\text{MesB-TCN}$ among these compounds, demonstrating the significant electron-deficient property of triarylboranes bearing a dicyanomethylene group. Density functional theory (DFT) calculations of $^{\text{F}}\text{MesB-TCN}$ and $\text{Mes}^*\text{B-TCN}$ were

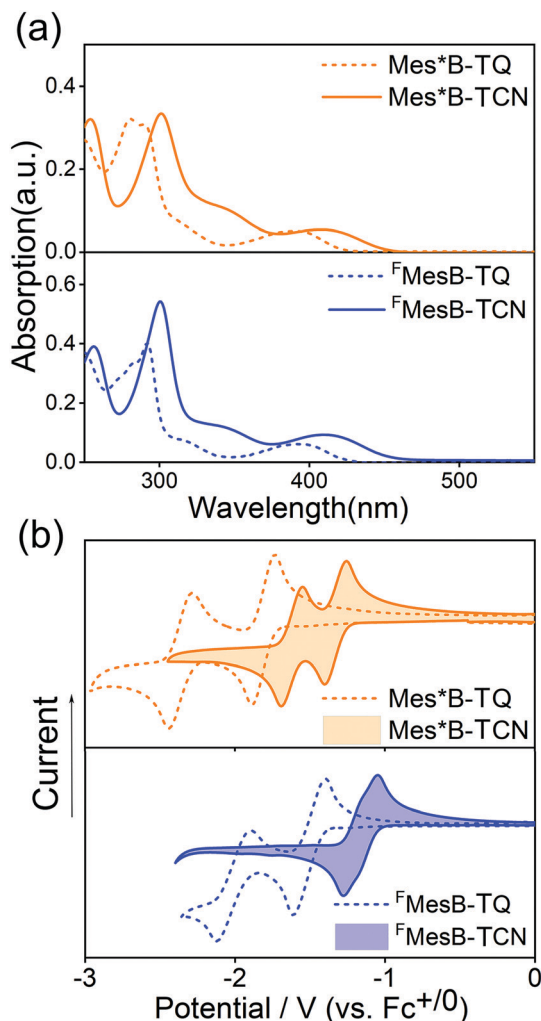


Fig. 2 (a) UV-Vis spectra (1×10^{-5} M) in THF and (b) cyclic voltammetry data of carbonyl- and dicyanomethylene-functionalized compounds in CH_2Cl_2 ($^{\text{F}}\text{MesB-TQ}$ and $^{\text{F}}\text{MesB-TCN}$) and THF ($\text{Mes}^*\text{B-TQ}$ and $\text{Mes}^*\text{B-TCN}$) with a scan rate of 100 mV s^{-1} .

conducted using the Gaussian 09 D.01 software package, and optimized geometries and single point energies were obtained at the B3PW91/6-311+G*/B3LYP/6-31G** level of theory. The plots of selected frontier orbitals are illustrated in Fig. S9 (ESI[†]) with the corresponding energy levels. The LUMOs of these compounds mainly localized on the boron-doped six-member ring and the dicyanomethylene group, and the LUMO energy levels are in good agreement with the energy levels estimated from CV data. TD-DFT calculations were also conducted at the

Table 1 Photophysical and electrochemical data of the dicyanomethylene-functionalized compounds

Compound	λ_{onset} (nm)	E_{g}^a (eV)	E_{red}^b (V)	LUMO ^c (eV)
$\text{Mes}^*\text{B-TCN}$	461	2.69	-1.33	-3.47
$^{\text{F}}\text{MesB-TCN}$	463	2.68	-1.19	-3.61

^a Optical gaps were estimated with the equation $E_{\text{g}} = 1240/\lambda_{\text{onset}}$. ^b Half-wave potentials of first reductive waves vs. $\text{Fc}^{+/0}$. ^c $E_{\text{LUMO}} = -(4.8 + E_{\text{red}})$.

PBE0/6-311+G* level of theory to get an in-depth understanding of the origins of the UV-vis absorption of the dicyanomethylene functionalized compounds, and the theoretical data match well with the experimental data (see Fig. S8 and S9 and Table S7, ESI† for details).

The solutions of these two compounds are almost non-emissive, but when we irradiate their solid powder with a UV lamp, ^FMesB-TCN exhibited a significant photoluminescence property with bright yellow-green fluorescence. This phenomenon cannot be observed in the neat film of ^FMesB-TCN, but can be repeated in block-shape crystal samples, as shown in Fig. 3a. The block single crystal of ^FMesB-TCN exhibited emission at 537 nm which showed a *ca.* 30 nm red-shift in comparison with the emission in solution ($\lambda_{em} = 508$ nm) and the neat film ($\lambda_{em} = 505$ nm). The photoluminescent quantum yield (PLQY) of the block single crystal of ^FMesB-TCN is *ca.* 33%, about 25 times higher than that in solution and the neat film (Fig. 3c and Table S4, ESI†), demonstrating a typical crystallization-induced emission enhancement (CIEE) behavior. Moreover, an acicular shape crystal of ^FMesB-TCN can be obtained *via* fast evaporation from its CH₂Cl₂ solution. Interestingly, the acicular shape crystal exhibited a different photo-luminescence property in comparison with the block shape crystal with much weaker and blue-shifted fluorescence ($\lambda_{em} = 504$ nm, PLQY = 1.3%). Powder X-ray diffraction (PXRD) measurements were performed on the highly emissive powder sample, which match well with the XRD peaks of the block crystal but are different to those of the acicular crystal. It demonstrated that the molecular packing mode in the powder samples is similar to that in the block crystals, which could be

the reason for the highly emissive property of the powder samples (see Fig. S2, ESI†). Further analysis of the molecular packing in the block single crystal of ^FMesB-TCN revealed a strong π - π interaction (3.296 Å, and 3.377 Å). On the contrary, the acicular crystal shows no significant π - π stacking interactions, as shown in Fig. 3b. It is unusual to see π - π stacking enhance the photoluminescence property, since strong π - π interactions between luminogens usually cause emission quenching.^{16,19} Several other intermolecular interactions can also be observed in the block crystal, *e.g.* N \cdots H-C interactions between cyano groups and naphthalene moieties (N \cdots H distance of 2.5–2.7 Å), and F \cdots H-C interactions between trifluoromethyl groups and naphthalene moieties (F \cdots H distance of *ca.* 2.53 Å), as shown in Fig. S3a (ESI†). Instead, much fewer interactions can be observed in the acicular crystals, mainly including C-H \cdots π interactions and F \cdots H-C interactions, as shown in Fig. S3b (ESI†). More intermolecular interactions in the block crystal mean that it has a more rigid molecular skeleton, which is usually favorable for radiative decay.

DFT calculations were conducted to study the electronic structures of the excited states of ^FMesB-TCN in the solid state (see the ESI† for details). Basically, the fluorescence of ^FMesB-TCN in the solid state can be assigned to the LUMO \rightarrow HOMO transition, and the electronic density contours of the HOMO and LUMO of the block and acicular crystals are plotted in Fig. S11 (ESI†). The corresponding electronic bandgaps of the block crystal and acicular crystal are 3.3171 eV and 3.3260 eV, respectively, explaining the bathochromic emission of the block crystal compared with the acicular crystal. The fluorescence quantum yield (Φ_F) is $\Phi_F \approx k_r/(k_r + k_{ic})$. k_r can

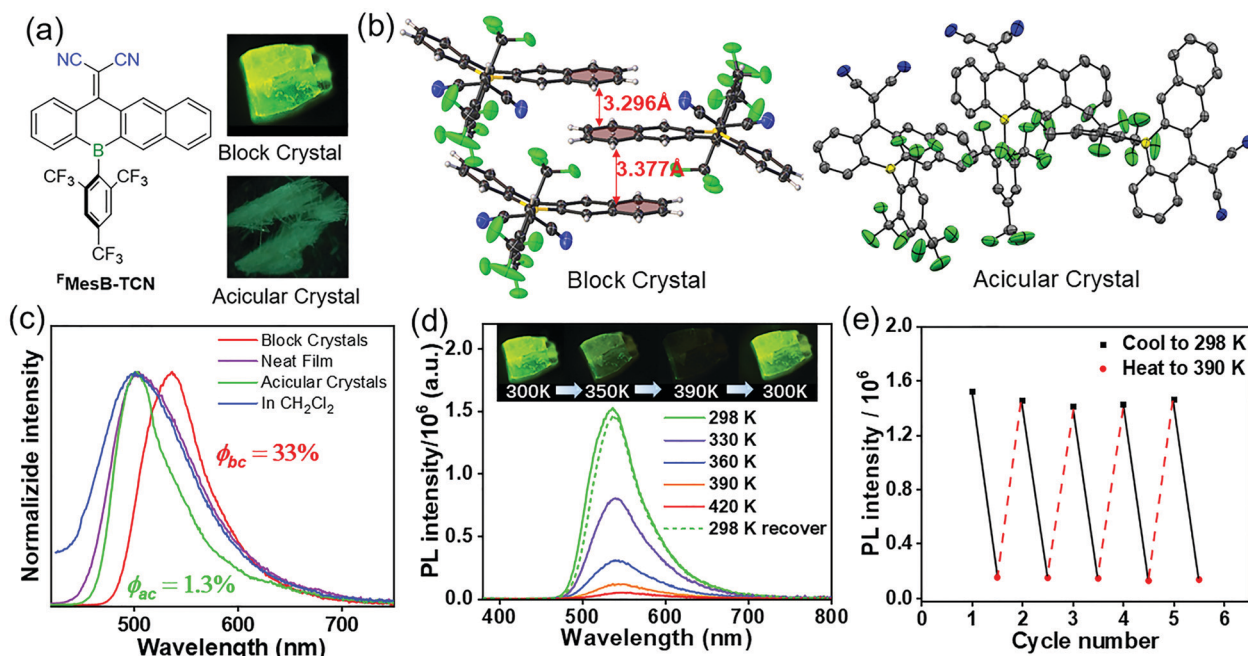


Fig. 3 (a) Fluorescence photos of the block crystal and acicular crystal of ^FMesB-TCN; (b) molecular packing structures of the ^FMesB-TCN block crystal and acicular crystal; (c) PL spectra of ^FMesB-TCN in different states with $\lambda_{ex} = 400$ nm; (d) PL spectra of the ^FMesB-TCN block single crystal at different temperatures with $\lambda_{ex} = 360$ nm, inset: fluorescence photos of the ^FMesB-TCN block single crystal at different temperatures; and (e) recycles of the PL intensity of ^FMesB-TCN (block crystal) at 540 nm as the temperature changed.

be estimated by simple spontaneous emission relationship $E \sim f\Delta E_{\text{vert}}^2$, where f is the dimensionless oscillator strength and ΔE_{vert} is the energy difference in units of cm^{-1} between the S_1 and S_0 states at the optimized S_1 geometry. As shown in Table S8 (ESI[†]), f and ΔE_{vert} for the block and acicular crystal are similar to each other. Therefore, the k_r values of the block and acicular crystals are similar to each other. The reorganization energy from S_0 to S_1 and *vice versa* can be obtained by the adiabatic potential (AP) energy surface method. We find that the total reorganization energy of the block crystal (430 meV) is smaller than that of the acicular crystal (450 meV), see Table S9 (ESI[†]). As known from previous work, the decrease of the reorganization energy can sharply retard the electron–vibration coupling caused nonradiative decay rate constant,^{23–27} thus, k_{ic} of the block crystal is smaller than that of the acicular phase. Therefore, the block crystal has a higher fluorescence quantum yield than the acicular crystal. Besides, the photo-luminescent properties of **Mes*B-TCN** in the block crystal, neat film and CH_2Cl_2 solution were also studied, and all these samples are weakly emissive, indicating that **Mes*B-TCN** exhibits no CIEE behavior (see Fig. S6 and Table S5, ESI[†]).

Moreover, the fluorescence intensity of the block single crystal of **F^rMesB-TCN** was dramatically quenched when the block single crystal was heated from 300 K to 420 K, as shown in Fig. 3d. Upon cooling the block crystal back to 300 K, the fluorescence can be recovered to the initial state, and this fluorescence switch cycle can be repeated at least 5 times without obvious fatigue (see Fig. 3e). Single crystal X-ray diffraction of the block crystal at 300 K and 400 K was conducted. From the result, an obvious change can be found in the molecular structure as shown in Fig. S4 (ESI[†]), which shows that the molecular structure at 300 K, including the main bond lengths and other parameters, is close to the single crystal diffraction data at 180 K, but the molecular structure at 400 K shows obvious deformation, which could affect the luminescence behavior of the molecules. Besides, the intermolecular interactions are also influenced by the increment of temperature with the π – π stacking distance changed from 3.296 Å and 3.377 Å at 300 K to 3.345 Å and 3.429 Å at 400 K, as shown in Fig. S5 (ESI[†]). Other interactions like $\text{N}\cdots\text{H}-\text{C}$ between cyano groups and naphthalene moieties also elongated from 2.649 Å at 300 K to 2.688 Å at 400 K. All these data revealed a more loose molecular packing of the block crystal at high temperature, which could result in enhanced non-radiative decay and quenching of fluorescence.

In this work, we reported a series of dicyanomethylene-bridged triarylboranes. The introduction of the dicyanomethylene group dramatically enhances the electron-deficient character with low-lying LUMO energy levels (< -3.5 eV), while retaining good stability. Interestingly, one of these compounds, **F^rMesB-TCN**, exhibits a crystallization-induced emission enhancement property, with a much higher PLQY (*ca.* 33%) of the block shape crystal than that of the solution, the neat film, and an acicular crystal from the same compound (*ca.* 1.3%). Single crystal X-ray diffraction indicated a much tighter packing mode in the block crystal with strong π – π interactions, which was not observed in the acicular crystal. DFT calculations revealed a smaller reorganization energy of the block crystal than

that of the acicular crystal, which matches well with the phenomenon of the highly emissive property of the block shape crystal. This work uncovered the structural and functional diversity of boron-containing molecules, while providing a new strategy for designing novel functional materials.

This work was funded by the National Natural Science Foundation of China (21772012, 21803007), and Beijing Institute of Technology Research Fund Program for Young Scholar. The authors acknowledge the Analysis and Testing Center of Beijing Institute of Technology for characterizations. G. M. L. also thanks the Project of the Science Funds of Jiangxi Education Office (GJJ180629) and the Project of Jiangxi Science and Technology Normal University (2016XJZD009) for financial support.

Conflicts of interest

There are no conflicts to declare.

Notes and references

- X. Cai and B. Liu, *Angew. Chem., Int. Ed.*, 2020, **59**, 9868–9886.
- Z. Guo, C. Yan and W. H. Zhu, *Angew. Chem., Int. Ed.*, 2020, **59**, 9812–9825.
- Q. Li and Z. Li, *Adv. Sci.*, 2017, **4**, 1600484.
- J. Ochi, K. Tanaka and Y. Chujo, *Angew. Chem., Int. Ed.*, 2020, **59**, 9841–9855.
- S. Suzuki, S. Sasaki, A. S. Sairi, R. Iwai, B. Z. Tang and G. I. Konishi, *Angew. Chem., Int. Ed.*, 2020, **59**, 9856–9867.
- S. Xu, Y. Duan and B. Liu, *Adv. Mater.*, 2020, **32**, e1903530.
- J. Yang, M. Fang and Z. Li, *Aggregate*, 2020, **1**, 6–18.
- X. Jin, M. B. Price, J. R. Finnegan, C. E. Boott, J. M. Richter, A. Rao, S. M. Menke, R. H. Friend, G. R. Whittell and I. Manners, *Science*, 2018, **360**, 897–900.
- H. B. Liu, J. L. Xu, Y. J. Li and Y. L. Li, *Acc. Chem. Res.*, 2010, **43**, 1496–1508.
- H. Shen, Y. Li and Y. Li, *Aggregate*, 2020, **1**, 57–68.
- D. Yan and D. G. Evans, *Mater. Horiz.*, 2014, **1**, 46–57.
- W. Zhang, J. Yao and Y. S. Zhao, *Acc. Chem. Res.*, 2016, **49**, 1691–1700.
- J. Mei, N. L. Leung, R. T. Kwok, J. W. Lam and B. Z. Tang, *Chem. Rev.*, 2015, **115**, 11718–11940.
- Z. Zhao, H. Zhang, J. W. Y. Lam and B. Z. Tang, *Angew. Chem., Int. Ed.*, 2020, **59**, 9888–9907.
- Y. Dong, J. W. Lam, A. Qin, Z. Li, J. Sun, H. H. Sung, I. D. Williams and B. Z. Tang, *Chem. Commun.*, 2007, 40–42.
- J. Tong, Y. J. Wang, Z. Wang, J. Z. Sun and B. Z. Tang, *J. Phys. Chem. C*, 2015, **119**, 21875–21881.
- H. Naito, K. Nishino, Y. Morisaki, K. Tanaka and Y. Chujo, *Angew. Chem., Int. Ed.*, 2017, **56**, 254–259.
- S. Yang, P. A. Yin, L. Li, Q. Peng, X. Gu, G. Gao, J. You and B. Z. Tang, *Angew. Chem., Int. Ed.*, 2020, **59**, 10136–10142.
- Y. Liu, A. Li, S. Xu, W. Xu, Y. Liu, W. Tian and B. Xu, *Angew. Chem., Int. Ed.*, 2020, **59**, 15098–15103.
- J. M. Wong, R. Zhang, P. Xie, L. Yang, M. Zhang, R. Zhou, R. Wang, Y. Shen, B. Yang, H. B. Wang and Z. Ding, *Angew. Chem., Int. Ed.*, 2020, **59**, 17461–17466.
- T. K. Wood, W. E. Piers, B. A. Keay and M. Parvez, *Angew. Chem., Int. Ed.*, 2009, **48**, 4009–4012.
- M. Mantina, A. C. Chamberlin, R. Valero, C. J. Cramer and D. G. Truhlar, *J. Phys. Chem. A*, 2009, **113**, 5806–5812.
- Y. Xie, T. Zhang, Z. Li, Q. Peng, Y. Yi and Z. Shuai, *Chem. – Asian J.*, 2015, **10**, 2154–2161.
- T. Zhang, Q. Peng, C. Quan, H. Nie, Y. Niu, Y. Xie, Z. Zhao, B. Z. Tang and Z. Shuai, *Chem. Sci.*, 2016, **7**, 5573–5580.
- X. Zheng, D. Wang, W. Xu, S. Cao, Q. Peng and B. Z. Tang, *Mater. Horiz.*, 2019, **6**, 2016–2023.
- X. Zheng, Q. Peng, L. Zhu, Y. Xie, X. Huang and Z. Shuai, *Nanoscale*, 2016, **8**, 15173–15180.
- Q. Peng, Y. Yi, Z. Shuai and J. S. Shao, *J. Am. Chem. Soc.*, 2007, **129**, 9333–9339.